Lab on a Chip

Cite this: *Lab Chip*, 2012, **12**, 2664–2671

www.rsc.org/loc

PAPER

Rapid protein concentration, efficient fluorescence labeling and purification on a micro/nanofluidics chip†

Chen Wang, Jun Ouyang, De-Kai Ye, Jing-Juan Xu, Hong-Yuan Chen and Xing-Hua Xia*

Received 10th October 2011, Accepted 13th April 2012
DOI: 10.1039/c2lc20977b

Fluorescence analysis has proved to be a powerful detection technique for achieving single molecule analysis. However, it usually requires the labeling of targets with bright fluorescent tags since most chemicals and biomolecules lack fluorescence. Conventional fluorescence labeling methods require a considerable quantity of biomolecule samples, long reaction times and extensive chromatographic purification procedures. Herein, a micro/nanofluidics device integrating a nanochannel in a microfluidics chip has been designed and fabricated, which achieves rapid protein concentration, fluorescence labeling, and efficient purification of product in a miniaturized and continuous manner. As a demonstration, labeling of the proteins bovine serum albumin (BSA) and IgG with fluorescein isothiocyanate (FITC) is presented. Compared to conventional methods, the present micro/nanofluidics device performs about 10^4–10^6 times faster BSA labeling with 1.6 times higher yields due to the efficient nanoconfinement effect, improved mass, and heat transfer in the chip device. The results demonstrate that the present micro/nanofluidics device promises rapid and facile fluorescence labeling of small amount of reagents such as proteins, nucleic acids and other biomolecules with high efficiency.

Introduction

Fluorescence analysis has proved to be a powerful and sensitive detection technique for reaching the single molecule level.[1–4] It is the method of choice for sensitive analysis in life sciences, environmental science, medicine and pharmacology, unraveling the inner workings of biomolecules, cells, and organisms. However, very few biomolecules can be directly visualized because of a lack of intrinsic fluorescence properties. Fluorescence labeling of biomolecules such as antibodies, proteins, amino acids and peptides provides an interesting and effective approach for the realization of bioanalysis with superior sensitivity.[5–7]

Conventional fluorescence labeling methods performed at the macroscale level use an excess of dye to achieve high labeling yields *via* covalent[8] or noncovalent interactions.[9] Noncovalent labeling relies on strong ionic, electrostatic, and hydrophobic interactions, and hydrogen bonding between the marker and biomolecules.[10] Although this method is relatively simple, it requires a multi-step staining protocol. In addition, the resultant products may lose their fluorescent tag after a long period of use. Covalent labeling can avoid the above problems *via* the formation of stable chemical bonds by the reaction of an appropriately functionalized dye marker with reactive groups on biomolecules. Covalent bond formation between the protein and fluorescein is highly specific, essentially irreversible, and occurs rapidly under physiological conditions. It is an ideal method of choice for labeling biomolecules. However, the conventional fluorescence labeling methods require a long reaction time, extensive chromatographic purification procedures to remove unreacted dye to minimize the background fluorescence, and a considerable quantity of the biomolecular sample. The latter issue becomes especially evident when the analyzed target is a rare and limiting resource in biological systems (for example, some kind of hormone, ligand, or antibody). Therefore, it is desirable and valuable to develop a miniaturized and more efficient labeling method that can perform fluorescence labeling at the nanogram or picogram scale.

Microfluidics technology offers advantages such as low reagent consumption, efficient reactions due to the high surface-to-volume ratio, reduced analysis time, and increased throughput. These attractive features make microfluidic devices promising as microreactors for biological reactions.[11–13] For example, Lee *et al.*[11] used electrophoretically mediated microanalysis (EMMA) to label proteins on-column with a fluorogenic reagent. Labeling was followed by capillary zone electrophoresis separation and postcolumn detection based on laser-induced fluorescence. Wheeler *et al.*[12] used a microfluidics chip to label biomolecules with radiometals. Their results demonstrated that the microreactors led to higher yields compared to identical reaction conditions in a bath system due to the improved mixing and heat transfer in the microfluidics system. Abdelgawad

State Key Laboratory of Analytical Chemistry for Life Science, School of Chemistry and Chemical Engineering, Nanjing University, Nanjing, 210093, China. E-mail: xhxia@nju.edu.cn; Fax: +86-25-83597436
† Electronic supplementary information (ESI) available. See DOI: 10.1039/c2lc20977b

et al.[13] reported the integration of digital microfluidics on the front end of a microchannel based system for labeling reactions and product separation. Although all these methods can perform labeling reactions in microsystems, external purification processes and relatively complicated chip designs for product purification are required.

Nanofluidics with downsized fluidic channels emerged at the end of 20th century and beginning of 21st century, and has grown rapidly to become an interesting new research field. To be considered nanofluidics, at least one of the dimensions must fall in the range of several to one hundred nanometers.[14] Compared to microfluidics devices, nanofluidics chips dominate the size and charge effects due to the nanoscaled space confinement. These attractive features make them promising as nanoreactors for biological reactions. Various applications including concentration of proteins and DNA,[15] enzymatic reaction kinetics assays,[16,17] cell assays,[18] single DNA analysis,[19] and immunoassays[20] have been achieved on nanofluidics devices. However, realization of concentration, reaction, and purification in one micro/nanofluidics device has not yet been proposed.

Herein, a micro/nanofluidics device that integrates a nanochannel in a microfluidics chip has been designed and fabricated. It was used to achieve rapid protein concentration, fluorescence labeling of targets and efficient purification of products in a miniaturized and continuous manner. A nanochannel on a polycarbonate (PC) plate is integrated into microfluidics chip on a polydimethylsiloxane (PDMS) slab to form a micro/nanofluidics device. The height of the nanochannel is size-tunable, ranging from several to tens of nanometers. The optimum height of the nanochannel allows small molecules to pass through while macromolecular proteins are efficiently concentrated before the nanochannel due to size and electrostatic effects. Using this micro/nanofluidics device, rapid protein concentration, fluorescence labeling of targets, and efficient purification of product can be accomplished. As a demonstration, labeling of the proteins bovine serum albumin (BSA) and IgG with fluorescein isothiocyanate (FITC) is presented. First, the negatively charged protein (BSA) is efficiently concentrated in front of the nanochannel under an electric field *via* the size effect and exclusion-enrichment effect (EEE).[16] As small molecule, the dye FITC (*ca.* 1 nm) is electrokinetically transported through the enriched BSA molecules, and the reactive derivative of the fluorophore selectively binds to the functional group of protein molecule *via* a covalent bond. This chemical reaction is illustrated in Scheme S1.† During the fluorescence labeling reaction, the unreacted dye molecules pass through the nanochannel by the electrokinetical driving force due to their smaller size, leaving purified labeled protein concentrated in front of the nanochannel. The micro/nanofluidics device and the processes for protein concentration, labeling reaction, purification, and detection are illustrated in Fig. 1. This micro/nanofluidics device performs all the processes of protein concentration, labeling, and purification in continuous manner without an external purification procedure on a chromatographic instrument to remove the unreacted dye. Especially importance is that the present device enables us to label reagents at the microgram or nanogram level, thus, providing a rapid, facile and highly sensitive approach to the fluorescence labeling of proteins, nucleic acids and other biomolecules.

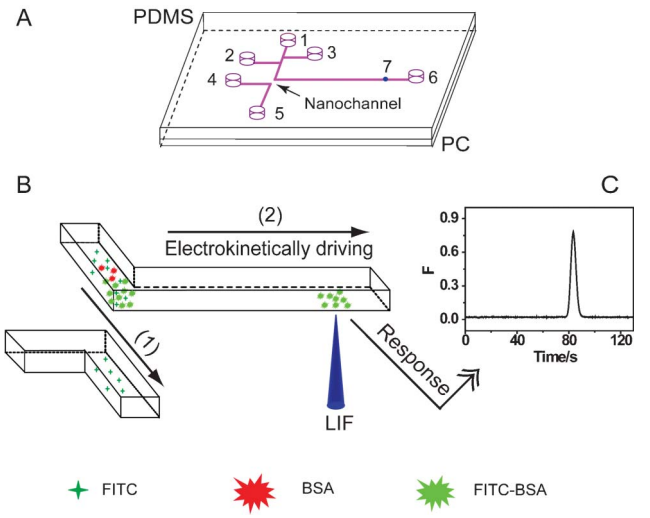

Fig. 1 (A) Schematic illustration of the micro/nanofluidics device for FITC labeling of protein. The nanogap is indicated by an arrow; (1) FITC reservoir; (2) BSA reservoir; (3–6) buffer reservoirs; (7) laser-induced fluorescence detection point. Total length 1–6 = 40 mm. (B) Schematic illustration of the principle for FITC labelling of proteins on the micro/nanofluidic device using bovine serum albumin (BSA) and fluorescein isothiocyanate (FITC) as model systems. (1) The electric field for protein concentration and FITC labeling; (2) the electric field for product separation and detection. (C) Corresponding fluorescence response of the purified product (FITC–BSA).

Experimental

Materials and reagents

Polycarbonate was from Suzhou Plastic Co. (Suzhou, China). PDMS base and curing agent were from Sylgard 184, Dow Corning, Midland, MI, USA. Fluorescein isothiocyanate labeled dog serum albumin (FITC–DSA) and fluorescein isothiocyanate (FITC) were obtained from Sigma. Bovine serum albumin (BSA), sodium bicarbonate, sodium carbonate and ammonium bicarbonate were purchased from Nanjing Chemical Reagent Company. Chemicals and solvents were of analytical grade and used as received. Bicarbonate buffer (BCB, pH 9.0, 20 mM) solution was used as the buffer system. All aqueous solutions were prepared from deionized water (18 MΩ cm^{-1}, PURELAB Classic, PALL, USA) and kept in a freezer to prevent deterioration. All liquid samples were filtered through a 0.22 μm syringe filter to remove particulates prior to use.

Micro/nanofluidics chip fabrication

The overall layout of the microfluidics device is represented in Fig. 1A. The nanochannel on PC was fabricated using the method we developed recently.[21] Briefly, a PC surface was exposed to 254-nm UV-light with a power density of 5 mW cm^{-2} in O_2 containing environments (*e.g.*, air). A commercially available poly(ethyleneterephthalate) (PET) film was used as the photomask because the PET film does not transmit UV-light with wavelengths ranging from 200 to 285 nm.[22] The profile of the etched region was recorded on a profilometer (Dektak 3, Veeco Inst Inc., USA). For fabrication of the microchannel on PDMS film, a PDMS base and curing agent were thoroughly

mixed in 10 : 1 ratio and directly cast over an SU-8 photoresist mold on a silicon substrate. The photoresist mold was fabricated by photolithography as previously described.[16] The PDMS was first allowed to rest at room temperature for 1 h to permit the removal of air bubbles. The device was then cured for 2 h at 70 °C. After cooling, the device was peeled off the master, cut to size and cleaned with methanol and deionized water. Then, the PDMS slab with microchannels and reservoirs was reversibly sealed to the PC plate with the nanochannel to form a complete micro/nanofluidics chip. The reversible bonding method can alleviate channel collapse and ensure better channel dimensions compared to the conventional thermal bonding approach. In the present work, the height of the nanochannel varied from 25 nm to 80 nm, the width was 100 μm, and the length was 100 μm. The dimensions of the microchannel were respectively 18 μm high and 100 μm wide. The total length of the micro/nanofluidic chip (1–6) was 40 mm. Reservoir 1 was filled with fluorescence reactant (FITC), reservoir 2 was filled with protein solution (*e.g.*, BSA), and remaining reservoirs were filled with buffer. Point 7 is the position for laser excitation and detection. The distance from the nanochannel point to the detection window was 28 mm.

Instrumentation

Fluorescence detection was carried out by a laser-induced fluorescence (LIF) detection system, as reported previously.[23] The light source comes from a 470-nm diode pumped laser (Changchun New Industries Optoelectronics Tech. Co., Changchun, China). Passed through a 470 nm band-pass filter (8-nm band-pass, Shenyang HB Optical Technology Co., Shenyang, China), the laser beam is reflected by a mirror and focused by a 40× microscope objective (0.65 NA, 3.0 mm long working distance, Chongqing MIC Optical & Electrical Instrument Co., Chongqing, China). Alignment of the micro/nanofluidics chip position was achieved by adjusting a translation stage (model TSM-4A-XYZ, Zolix Instruments Co., Beijing, China). The fluorescence light transmitted through the chip was collected by a 25× microscope lens (Xi'an Sicong Laser Co., Xian, China), and was detected by a photomultiplier tube (PMT R928, with an integrated amplifier CC171, Hamamatsu, Japan) after being transmitted through a 510-nm long-pass filter and a 525 nm band-pass filter (15-nm band-pass, Shenyang HB Optical Technology Co.). The output signals from the PMT were recorded on a personal computer *via* an AD/DA converter. The fluorescence microscope investigation was performed using an inverted fluorescence microscope (Leica, Dmire2, Germany) equipped with a highly sensitive CCD color video camera (S45, Canon, Japan). NIS-elements BR 2.30 software (Nikon) was used for camera control and image processing. A laboratory-made high voltage power supply (0–5000 V) was used to apply electric fields to the microchannels through platinum electrodes placed in the reservoirs. The applied voltage can be automatically controlled by a personal computer *via* an AD/DA converter. The current was monitored in real time and the corresponding data saved in text files.

Protein concentration, labeling, and purification on the miro/nanofluidics device

Protein concentration, labeling, and purification were carried out subsequently on the micro/nanofluidics device, as shown schematically in Fig. 1. In this work, reservoir 1 was filled with the fluorescence reactant (FITC), reservoir 2 was filled with BSA, and the remaining reservoirs were filled with buffer. The protein concentration experiments were carried out as described previously.[16] Briefly, running buffer was first introduced into all the reservoirs and then to fill all the channels by squeezing slightly the buffer solution in the channels. After that the protein (BSA in 20 mM BCB, pH 9.0) solution was introduced into the protein reservoir (reservoir 2), and Pt electrodes were placed the in reservoirs. First, 400 V potential was applied between reservoirs 2 and 5 for electrokinetic enrichment of the protein BSA. Then, the voltage was changed to reservoir 1 and 5 for transporting FITC through the enriched BSA for the labeling reaction. After the reaction proceeded for a period of time, buffer (instead of FITC solution) was driven through the channels for product purification. Collection of the product (fluorescein isothiocyanate labeled protein, FITC–BSA) was carried out by applying 1000 V separation voltage between reservoirs 3 and 6. The labeled protein was detected by a LIF detector as shown in Fig. 1B. Point 7 is the position for the laser excitation and detection. The distance from the nanochannel point to the detection window was 28 mm. To avoid nonspecific adsorption of protein and dye to the channel walls, and therefore an alteration to the electroosmotic mobility, the surface of the channel walls was modified as reported before.[24] First, a mixture of $H_2O/H_2O_2/HCl$ (in a volume ratio of 5 : 1 : 1) was continuously passed through the microchannels for 5 min, followed by flushing with deionized water. Then, PEG (3% solution) was introduced into the microchannels and incubated for several hours for each new microchip. They were then flushed with buffer solution until the current of the power supply became level. To avoid the presence of side and degradation products in the micro/nanofluidics chip, the FITC solution was prepared freshly prior to use.

Conventional fluorescence labeling of protein in bulk solution

A mixture of 6 μg ml^{-1} of the dye FITC and 100 μg ml^{-1} of BSA were prepared in BCB buffer (20 mM, pH 9.0), and then stored at 25 °C in the dark for incubation overnight.[25] After different reaction times, the protein–dye conjugates were separated from an excess of dye using size exclusion chromatography on a Sephadex G25 medium column (GE Healthcare) with BCB buffer as the eluent. The labeling reaction kinetics were monitored by following the changes in the UV–vis absorbance of purified FITC–BSA as a function of time.

Calculation of the dye-to-protein ratio (DPR)

A series of BSA and FITC solutions with different concentrations were prepared in 20 mM BCB (pH 9.0) to establish the calibration graphs. The intrinsic absorbance of BSA is at 280 nm and FITC at 495 nm. To obtain the dye-to-protein ratio (DPR), the absorbance intensity ratio of dyes to conjugates was determined on a UV-3600 UV–vis spectrometer (Shimadzu, Japan).

Safety considerations

The high-voltage power supply should be handled with extreme care to avoid electric shock.

Results and discussion

Optimization of nanochannel height for protein concentration

For protein concentration, labeling, and purification, the micro/nanofluidics chip should have the capacity for efficient protein concentration, fast reaction times, and complete purification. In an ideal case, protein and labeled protein can be concentrated in front of the nanochannel and the unreacted labeling molecule is transported through the nanochannel. As discussed previously,[26,27] mass transfer (J) across a nanochannel along the x-axis is governed by the Nernst–Planck equation (eqn (1)).

$$J(x) = -D\frac{\partial C(x)}{\partial x} - \frac{zF}{RT}DC\frac{\partial \varphi(x)}{\partial x} + Cv_{eo}(x) \quad (1)$$

where D, C, and z are the diffusion coefficient, concentration, and charge of the permeation species, respectively. $\partial C(x)/\partial x$ is the concentration gradient at distance x, $\partial \phi(x)/\partial x$ is the potential gradient, and v_{eo} is the electroosmotic velocity. The three terms on the right-hand side of eqn (1) represent the contributions of diffusion, electromigration, and electroosmotic flow. In the present case, since external voltage is applied to the nanochannel, mass transport driven by diffusion due to concentration gradient can be neglected as compared to other two terms. For a negatively charged channel (*e.g.*, under the conditions in the present study), the electroosmotic flow moves the liquid along the direction of electric field; while the electromigration moves the negatively charged species against the direction of electric field. Since the electroosmotic flow rate is much faster than the electromigration rate (usually by more than 3 times), the negatively charged species is transported along the direction of electric field. However, if the nanochannel size decreases to values comparable to the double layer thickness or the size of transported species, the mass transport will be predominantly determined by steric hindrance and electrostatic interactions.[27,28] As illustrated in Fig. 2, the nanochannel for mass transport can be divided into an electrostatic interaction region and a free transport region. Since the nanochannel surface carries negative charges in this study, transport of cations is permitted; while transport of anions is blocked due to the electrostatic interactions, resulting in the concentration of anions in front of the nanochannel. This ionic selective "exclusion-enrichment effect" is simplified as "charge-effect" in this work. On the other hand, mass transport in the free transport region is assumed to be the same as in the bulk system if the size of the transported species is smaller than the width of the free transport region; otherwise transport is blocked due to steric hindrance. This phenomenon is referred to as the "size effect". When the solution pH and the concentration of the buffer are kept constant, the electrical double layer (EDL) thickness can be assumed to be constant; therefore, the mass transport is mainly determined by the alteration of free transport region, *e.g.*, nanochannel size.

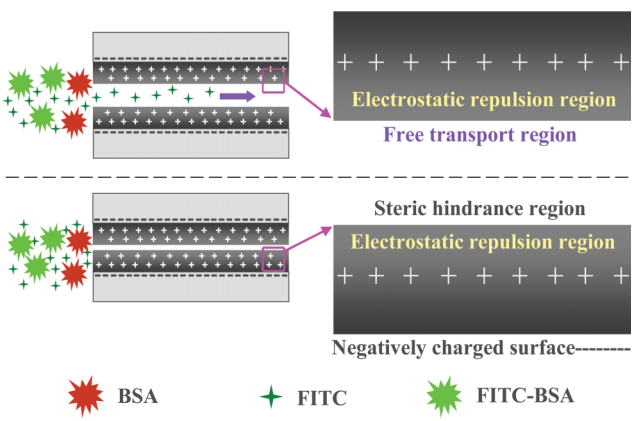

Fig. 2 Schematic representation of the working principle for protein concentration, labeling, and purification using the nanochannel.

In BCB buffer (pH 9.0), FITC, DSA and FITC–DSA are all negatively charged. The averaged hydrodynamic diameter of FITC–DSA is 7.25 nm as determined by dynamic light scattering (BI-200SM, BIC, America). The molecular size of FITC is less than 1 nm, and the size of DSA should be comparable to FITC–DSA. Due to the different charge and size of FITC, DSA and FITC–DSA, the simultaneous concentration of proteins in front of the nanochannel and free transport of FITC through the nanochannel can be realized if the nanochannel height is properly chosen.

To realize the optimal performance of the present micro/nanofluidics device, nanochannels with different heights were prepared. As we reported previously,[21] the etching rate is *ca.* 0.015 nm s^{-1} in our experiment conditions. Therefore, nanochannels on PC with height of about 72, 63, 45, 36 and 27 nm were prepared using a UV irradiation time of 80, 70, 50, 40, 30 min, respectively. Typical profiles of the etched nanochannels are shown in Fig. S1.† Channel collapse may exist due to the large value of depth-to-width ratio (from 1 : 4000 to 1 : 1250) after the reversible bonding of the PDMS slab to the PC plate. In our experiments, no electrical current flowed through the nanochannel when the UV-irradiation time was less than 20 min. This indicates that the nanochannel is completely blocked due to nanochannel collapse. When the UV-irradiation time reached 30 min, a small electrical current appeared, indicating the existence of a nanochannel. Therefore, the real nanochannel depth is likely to be smaller than the values determined by profilometer in the micro/nanofluidics chip.

In the protein concentration experiments, FITC labeled protein (FITC–DSA) and FITC were individually used to determine the optimal height of nanochannel. The results in Fig. 3 show clearly that the nanochannel height significantly influences the concentration of protein and FITC samples. For both samples, the enrichment effect becomes weaker with increases in the nanochannel height. However, there is a distinct difference in the concentration phenomenon between FITC–DSA and FITC due to the considerable difference in their sizes. As expected, the FITC–DSA sample can be more easily concentrated in front of the nanochannels at the anodic side as compared to the FITC molecules. As shown in Fig. 3A, obvious concentration of FITC can only occur with UV-irradiation time of 30 min (photo e). With the increase of UV-irradiation time to 40 min, only slight concentration of FITC occurred (photo d). Further increases to the nanochannel height resulted in no FITC concentration (photos a–c). In contrast, obvious concentration of FITC–DSA was observed with UV-irradiation times from 30 to 50 min (Fig. 3B, photos c–e). Even at UV-irradiation times as long as 80 and 90 min, a slight concentration of FITC–DSA was

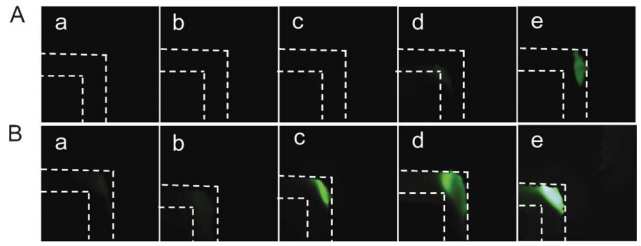

Fig. 3 The photographs of 6 μg ml^{-1} FITC in 20 mM BCB buffer (pH 9.0) (A), and 100 μg ml^{-1} FITC–DSA in 20 mM BCB buffer (pH 9.0) (B) in the micro/nanofluidics device with different nanochannels (a–e, corresponding to irradiation times of 80, 70, 50, 40, and 30 min, respectively). Images were taken after applying a voltage of 400 V between the FITC (1) or protein reservoir (2) and waster reservoir (5) as indicated in Fig. 1A for 300 s, respectively. Dotted lines indicate the outlines of the microchannels.

visible (Fig. 3B, photos a and b). These phenomena can be understood if we consider both the charge effect and size effect. As mentioned above, the real nanochannel height could be smaller than the values determined by profilometer. The double layer thickness is about 2.15 nm for 20 mM phosphate buffer (PBS) as calculated using a finite element model in our previous report.[27] (In reality, the charge effect region should be larger than the calculated double layer thickness.) If the smallest size of the nanochannel is less than 4.3 nm in height, the double layer overlaps in the nanochannel and transport of co-ions (the same charge as the surface charge) in the nanochannel will be blocked. Thus, concentration of the co-ions in front of the nanochannel occurs due to electrostatic interactions. FITC and FITC–DSA molecules are all negatively charged in this work and they can both be efficiently concentrated in front of the nanochannel prepared using 30 min irradiation time because of the charge-effect and size-effect. However, when the height of the nanochannel is larger than twice the thickness of the double layer, a free transport region outside the EDL exists. Therefore, if the size of molecules is slightly smaller than the free transport region, some of the co-ions (the same charge as the surface) will be transported through the nanochannel and some of the co-ions will accumulate in front of the nanochannel due to the limited transport rate. However, with further increases in the channel size, more and more molecules can be transported through the nanochannel, and the concentration effect becomes weak. This ionic selectivity effect is caused by varying the nanochannel height. The results in Fig. 3 demonstrate that the micro/nanofluidics device with the nanochannel fabricated by 50 min UV-irradiation of the PC surface is of a reasonable size to achieve protein concentration, labeling and purification. In this case, protein and FITC–DSA conjugates can be efficiently concentrated by 10^3–10^4 fold, while the small dye molecule can freely pass through the nanochannel.

For protein concentration, labeling, and purification, the negatively charged BSA (100 μg ml^{-1}) was concentrated at the anodic electrode side of the nanochannel by applying a high voltage (400 V) to the reservoirs (2, anode) and (5, cathode) in Fig. 1A. After 300 s of protein concentration, the direction of the electric field was changed to the reservoirs (1, anode) and (5, cathode), so that the small molecule FITC (6 μg ml^{-1}) was electrokinetically transported through the enriched proteins for 600 s during which the fluorescence labeling reaction and purification proceeded simultaneously. The reactive derivative of FITC selectively reacted with the functional group of protein to form FITC–BSA conjugates and excess FITC was transported across the nanochannel continuously. In order to obtain FITC labeled BSA with high purity, further purification was essential. Thus, buffer was driven through the nanochannel by application of a high voltage (400 V) to reservoirs (3, anode) and (5, cathode) to remove the unreacted FITC molecules. The results are shown in Fig. 4. First, fluorescence appears at both sides of the nanochannel (Fig. 4A(a)), indicating removal of the unreacted FITC molecules from the labeling reaction region. After a period of time (60–70 s) the fluorescence intensity became weak due to the gradual removal of the unreacted FITC molecules (Fig. 4(b) and (c)). After purification for 90 s (Fig. 4(d)), no fluorescence appeared at the negative side of the nanochannel due to the complete removal of FITC, indicating that purification of the fluorescence labeled protein was finished. Subsequent collection and detection of labeled proteins can be easily achieved by switching the electric field to reservoirs (3, anode) and (6, cathode) for microchip separation and laser-induced fluorescence detection at excitation emission wavelengths of 470/525 nm. The appearance of a highly purified product peak at about 83 s in Fig. 4B further confirms that labeling and purification of protein can be easily achieved in the present micro/nanofluidics chip.

Optimization of labeling conditions

The influence of solution pH on the labeling reaction efficiency was considered since the solution pH will change the surface charges of proteins, FITC and the channel, and possibly alter the conformation of proteins. Solutions of BSA (100 μg ml^{-1}) and FITC (6 μg ml^{-1}) in 20 mM BCB buffer with pH 8.5, 9.0, 9.5 and 10.0 were prepared. Protein concentration, labeling and purification processes were performed on the micro/nanofluidics chip under the conditions of 300 s BSA concentration, 600s FITC labeling reaction and 90 s buffer purification, followed by microchip electrophoresis separation at 1000 V and LIF detection. As shown in Fig. S2,† the fluorescence intensity increased with an increase in the solution pH. However, it is

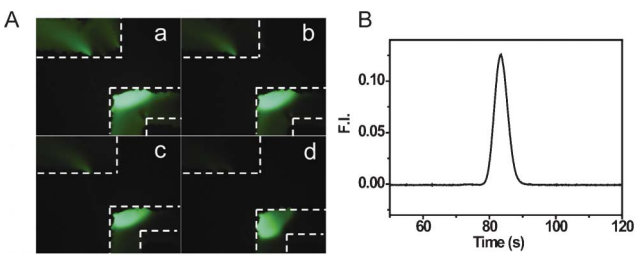

Fig. 4 (A) Time sequence photo images (a–d) showing purification of the FITC–BSA conjugates formed on the micro/nanofluidic device. Images were taken after buffer (instead of FITC solution) was electrokinetically driven through the nanochannel for 30, 60, 70, and 90 s, respectively. (B) Micro/nanofluidics chip electropherogram of BSA labeled on-chip with FITC. Protein concentration time: 300 s; FITC flowing (labeling) time: 600 s; purification time: 90 s. Separation voltage: 1000 V applied at reservoirs 3 (anode) and 6 (cathode) as indicated in Fig. 1A. Dotted lines indicate the outlines of the microchannels.

known that if the solution pH is too high it may change the conformation and bioactivity of biomolecules. In addition, hydrolysis of FITC is a base catalyzed reaction, and hydrolysis becomes more significant at higher pH values. Thus, a solution of pH 9.0 should be a reasonable value for a satisfactory labeling reaction.[29]

The influence of protein concentration on the labeling reaction efficiency was also investigated since the concentration also determines the labeling reaction kinetics. The concentration of proteins in front of the nanochannel can be increased by increasing the concentration time. The results are shown in Fig. S3.† The peak at 83 s is related to FITC–BSA, and the peak at 103 s corresponds to FITC. It is clear that when the BSA concentration time is below 300 s there is a single peak at 83 s in the electropherograms, indicating purified FITC–BSA. The peak height at 83 s increased with the protein concentration time, indicating that more reaction product was formed with longer concentration time. However, when the BSA concentration time reached 450 s, a second peak at 103 s appeared, indicating that unreacted FITC could not be completely removed using the same purification time. This phenomenon can be explained by the difference of the concentrated protein quantity in front of the nanochannel. When the protein quantity is small (enrichment time less than 300 s), FITC can freely pass through the gaps between proteins to reach the nanochannel, and unreacted FITC will not be accumulated. However, when the protein enrichment time is prolonged, a large quantity of enriched protein may result in smaller gaps between proteins, decreasing the transport rate of FITC or even blocking the FITC from reaching the nanochannel. In this case, a longer purification time is required to obtain pure reaction product FITC–BSA.

Comparison of the labeling reaction kinetics in micro/nanofluidics chip and in bath system

In order to understand the labeling reaction kinetics, the protein concentration time of 300 s from BSA solution (100 μg ml^{-1}, 1.5 nM, pH 9.0) was used. FITC solution (6 μg ml^{-1}, 15 nM, pH 9.0) was then electrokinetically driven through the concentrated proteins for the labeling reaction at room temperature. Varied labeling reaction times were followed by 90 s purification, separation and detection of the product FITC–BSA. The results are shown in Fig. 5A. The fluorescence intensity of the product increased sharply within the first 300 s, then reached a plateau. This demonstrates that the labeling reaction in the micro/nanofluidics chip occurs within the first 500 s. The trend indicates that the reaction is finished after 750 s reaction time. With the continuous flow of FITC through the reaction region, the FITC concentration can be considered constant. The labeling reaction of the concentrated BSA is assumed to be completed at the reaction time of 750 s, and thus, the final concentration of BSA can be considered as 0 nM after 750 s. The initial concentration of BSA enriched in front of the nanochannel can be considered a constant value, the concentration of BSA at different reaction time can thus be calculated from the fluorescence change of the product FITC–BSA. A plot of the natural logarithm of reactant BSA concentration (ln$C$) as a function of reaction time (t) results in a linear relationship (Fig. 5B), which is a typical characteristic of a first-order reaction. From the slope of this line (the correlation coefficient: 0.9965), the effective rate constant (k) for the labeling reaction was calculated to be 0.0065 s^{-1}.

For comparison, the labeling reaction of proteins in a bath solution system was also carried out. In this experiment, FITC solution was added into a BSA solution (100 μg ml^{-1}, 1.5 nM) to reach a FITC concentration of 6 μg ml^{-1} (15 nM). After the labeling reaction occurred in the dark for different times, the reaction product was sampled and purified using a NAP™-5 (Sephadex™ G-25) column, and then detected using UV-vis absorbance spectroscopy. The results are shown in Fig. S4 and S5.† It is clear that a much longer labeling reaction time is needed to reach the plateau as compared to the reaction performed in the micro/nanofluidic chip. Plotting the natural logarithm of protein (BSA) concentration (ln$C$) as a function of reaction time resulted in a linear line, demonstrating the same first-order reaction kinetics for the BSA labeling reaction in the bath system. The calculated effective reaction rate constant (k) is only 9.78 × 10^{-5} s^{-1}, which is 66.5 times slower than that in the micro/nanofluidic chip (0.0065 s^{-1}). Since the protein concentration is about 10^3–10^4 fold higher than in bath system, the maximum reaction rate would be 10^4–10^6 fold faster in the micro/nanofluidic chip than in bath system.

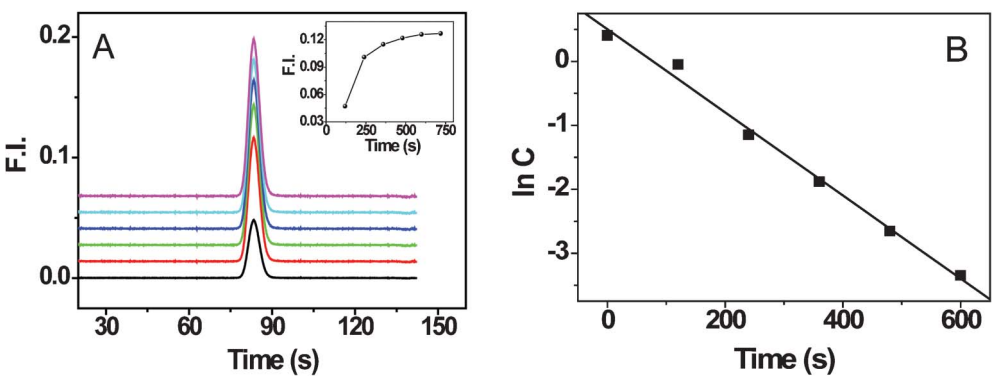

Fig. 5 (A) Electropherograms of the purified FITC–BSA product obtained from different labeling reaction time on the micro/nanofluidics chip. Labeling reaction time (from bottom to top): 120, 240, 360, 480, 600, and 720 s. BSA (100 μg ml^{-1}) concentration time: 300 s. Other experimental conditions: solution pH 9.0, temperature 25 °C, separation voltage: 1000 V. The inset is a plot of fluorescence intensity of FITC–BSA *versus* FITC flowing time (reaction time). (B) Plot of the natural logarithm of protein (BSA) concentration (ln$C$) as a function of reaction time (t). The data were obtained from (A).

The dye-to-protein ratio (DPR) is the average number of chromophores conjugated to a single protein molecule, characterizing the fluorescence labeling yield and the fluorescence intensity of labeled protein. The DPR value can be obtained from the UV–vis absorbance assays for BSA at 280 nm and FITC at 495 nm. When we measured the absorbance intensity of the labeled FITC–BSA at 280 nm, one has to consider the contribution from FITC since it shows a weak absorbance at the same wavelength (Fig. S6†) besides its main absorbance at 495 nm. By subtracting the background signal, it was found that the absorbance of FITC at 280 nm is approximately one third of the main absorbance at 495 nm ($A280 = A495/3$). The DPR for different reaction times in the bath system was determined from the UV–vis spectra (Fig. S4†) based on calibration curves of BSA and FITC (Fig. S6 and S7†), as shown in Fig. S8.† It clearly shows that the fluorescence labeling yield increases with the reaction time and then reaches a maximum value of 1.51 after a reaction time of 14 h. For comparison, the DPR for the labeling reaction in the micro/nanofluidics device was also investigated. Fig. S9† shows the UV–vis spectra of the product FITC–BSA synthesized from the micro/nanofluidics device for 720 s and from the conventional bath system for 14 h. The calculated DPR value in micro/nanofluidics chip is 2.48, which is higher than the value of 1.51 from the bath system. The results show that improved mixing and heat transfer in the micro/nanofluidics device lead to higher yields in addition to a faster labeling reaction rate for identical reaction conditions.

Extending the present approach to the labeling of other proteins and dyes

The fluorescent labeling reaction performed by the present micro/nanofluidics device is not specific to BSA, but can be extended to the fluorescence labeling of other proteins (*e.g.*, immunoglobulin G, IgG) and the use of other dyes. Fig. S10† shows the electropherograms of IgG labeled with FITC on the micro/nanofluidics chip in pH 9.0 BCB solutions at room temperature. A purified electropherogram peak clearly appeared at *ca.* 80 s for the labeling product FITC–IgG, demonstrating successful FITC labeling of IgG. In principle, labeling of other proteins can also be achieved on this micro/nanofluidics device. In addition, this micro/nanofluidics device is not only limited to FITC, but can also be used for protein labeling with other small molecule dyes providing the size of the nanochannel is tuned properly. To confirm this idea, we performed an additional experiment using Rhodamine B isothiocyanate (RBITC), a positively charged dye. In this case, the "charge-effect" of the nanochannel is used for protein labeling. The nanochannel size is tuned to values comparable to the EDL thickness, so that the EDL overlaps completely. Under the action of the electrical field, negatively charged protein is efficiently concentrated in front of the nanochannel, while the positively charged dye can easily pass through the enriched proteins and nanochannel due to the "exclusion-enrichment effect" of the nanochannel. Thus, protein labeling can be realized in a continuous manner in the chip. The other reaction conditions were the same as for FITC labelling. The results in Fig. S11† shows the excellent ability of this device for protein labeling with other dyes.

Conclusion

In summary, we have designed a novel micro/nanofluidics device integrated with a nanochannel, chip electrophoresis and a laser induced fluorescence detector. This device can perform multiple functions in a continuous manner, including the highly efficient concentration of proteins by making use of the charge and size effects, fluorescence labeling reaction of the concentrated proteins, product purification, and product collection with laser induced fluorescence detection. Due to the efficient nanoconfinement effect, improved mass and heat transfer in the micro/nanofluidic device as compared to the conventional bath system, the fluorescence labeling reaction rate in the present micro/nanofluidics device is about 10^4–10^6 times faster and the labeling yield is about 1.6 times higher. In addition, this device allows highly efficient fluorescence labeling at the micro-/nano-gram scale and is not specific to BSA. This micro/nanofluidic device can accelerate the labeling time, increase labeling efficiency, and minimize the total cost. The present work promises a simple, rapid, and highly efficient approach for the fluorescence labeling of proteins, nucleic acids and other biomolecules. We anticipate this micro/nanofluidics system will find wide applications in the fields of chemistry, life science, and materials sciences.

Acknowledgements

This work was supported by grants from the National 973 Basic Research Program (2012CB933804), the National Natural Science Foundation of China (NSFC, No. 21035002, 20890020, 20975047), the National Science Fund for Creative Research Groups (21121091), and the Natural Science Foundation of Jiangsu province (BK2010009).

References

1 S. A. Soper, E. B. Shera, J. C. Martin, J. H. Jett, J. H. Hahn, H. L. Nutter and R. A. Keller, *Anal. Chem.*, 1991, **63**, 432–437.
2 C. Gooijer, S. J. Kok and F. Ariese, *Analusis*, 2000, **28**, 679–685.
3 M. Lacroix, V. Poinsot, C. Fournier and F. Couderc, *Electrophoresis*, 2005, **26**, 2608–2621.
4 D. Y. Chen and N. J. Dovichi, *Anal. Chem.*, 1996, **68**, 690–696.
5 H. Mader, X. H. Li, S. Saleh, M. Link, P. Kele and O. S. Wolfbeis, *Ann. N. Y. Acad. Sci.*, 2008, **1130**, 218–223.
6 I. L. Medintz, H. T. Uyeda, E. R. Goldman and H. Mattoussi, *Nat. Mater.*, 2005, **4**, 435–446.
7 B. K. Wetzl, S. M. Yarmoluk, D. B. Craig and O. S. Wolfbeis, *Angew. Chem., Int. Ed.*, 2004, **43**, 5400–5402.
8 A. V. Stoyanov, H. Ahmadzadeh, S. N. Krylov and B. J. Chromatogr, *Anal. Chem.*, 1998, **70**, 2493–2494.
9 (*a*) R. J. Williams, M. Lipowska, G. Patonay and L. Strekowski, *Anal. Chem.*, 1993, **65**, 601–605; (*b*) M. D. Harvey, V. Bablekis, P. R. Banks and C. D. Skinner, *J. Chromatogr., Biomed. Appl.*, 2001, **754**, 345–356.
10 G. Patonay, J. Salon, J. Sowell and L. Strekowski, *Molecules*, 2004, **9**, 40–49.
11 I. H. Lee, D. Pinto, E. A. Arriaga, Z. U. Zhang and N. J. Dovichi, *Anal. Chem.*, 1998, **70**, 4546–4548.
12 T. D. Wheeler, D. X. Zeng, A. V. Desai, B. Önal, D. E. Reichert and P. J. A. Kenis, *Lab Chip*, 2010, **10**, 3387–3396.
13 M. Abdelgawad, M. W. L. Watson and A. R. Wheeler, *Lab Chip*, 2009, **9**, 1046–1051.
14 A. Patrick and T. N. Nam, *Anal. Chem.*, 2008, **80**, 2326–2341.
15 (*a*) H. Yu, Y. Lu, Y. G. Zhou, F. B. Wang, F. Y. He and X. H. Xia, *Lab Chip*, 2008, **8**, 1496–1501; (*b*) H. Cui, K. Horiuchi, P. Dutta and C. F. Ivory, *Anal. Chem.*, 2005, **77**, 1303–1309; (*c*) D. Akin, H. Li and R. Bashir, *Nano Lett.*, 2004, **4**, 257–259; (*d*) A. Patrick and T. N. Nam, *Anal. Chem.*, 2008, **80**, 2326–2341.

16 (*a*) C. Wang, S. J. Li, Z. Q. Wu, J. J. Xu, H. Y. Chen and X. H. Xia, *Lab Chip*, 2010, **10**, 639–646; (*b*) S. J. Li, C. Wang, Z. Q. Wu, J. J. Xu, X. H. Xia and H. Y. Chen, *Chem.–Eur. J.*, 2010, **16**, 10186–10194.
17 J. H. Lee, Y. A. Song, S. R. Tannenbaum and J. Han, *Anal. Chem.*, 2008, **80**, 3198–3204.
18 J. H. Lee, B. D. Cosgrove, D. A. Lauffenburger and J. Han, *J. Am. Chem. Soc.*, 2009, **131**, 10340–10341.
19 P. Sivanesan, K. Okamoto, D. English, C. S. Lee and D. L. Devoe, *Anal. Chem.*, 2005, **77**, 2252–2258.
20 T. Endo, K. Kerman, N. Nagatani, H. M. Hiepa, D. Kim, Y. Yonezawa, K. Nakano and E. Tamiya, *Anal. Chem.*, 2006, **78**, 6465–6475.
21 (*a*) C. Wang, J. Ouyang, H. L. Gao, H. W. Chen, J. J. Xu, X. H. Xia and H. Y. Chen, *Talanta*, 2011, **85**, 298–303; (*b*) C. Wang, Z. H. Sheng, J. Ouyang, J. J. Xu, H. Y. Chen and X. H. Xia, *ChemPhysChem*, 2012, **13**, 762–768.
22 Y. Kong, H. W. Chen, X. Yun, Z. X. Hao and Z. L. Fang, *Chin. J. Anal. Chem.*, 2007, **35**, 623–627.
23 J. L. Fu, Q. Fang, T. Zhang, X. H. Jin and Z. L. Fang, *Anal. Chem.*, 2006, **78**, 3827–3834.
24 G. D. Sui, J. Y. Wang, C. C. Lee, W. X. Lu, S. P. Lee, J. V. Leyton, A. M. Wu and H. R. Tseng, *Anal. Chem.*, 2006, **78**, 5543–5551.
25 (*a*) J. D. Marshall, W. C. Eveland and C. W. Smith, *Proc. Soc. Exp. Biol. Med.*, 1958, **98**, 898–900; (*b*) W. W. Bromer, S. K. Sheehan, A. W. Bems and E. R. Arquilla, *Biochemistry*, 1967, **6**, 2378–2388.
26 W. Chen, J. H. Yuan and X. H. Xia, *Anal. Chem.*, 2005, **77**, 8102–8108.
27 W. Chen, Z. Q. Wu, X. H. Xia, J. J. Xu and H. Y. Chen, *Angew. Chem., Int. Ed.*, 2010, **49**, 7943–7947.
28 S. J. Li, J. Li, K. Wang, C. Wang, J. J. Xu, H. Y. Chen, X. H. Xia and Q. Huo, *ACS Nano*, 2010, **4**, 6417–6424.
29 S. K. Lau, F. Zaccardo, M. Little and P. Banks, *J. Chromatogr., A*, 1998, **809**, 203–210.